Postprint of: Chróścielewski J., Lubowiecka I., Szymczak Cz., Witkowski W., On some aspects of torsional buckling of thin-walled I-beam columns, Computers & Structures, Vol. 84, Iss. 29–30 (2006), pp. 1946-1957, DOI: 10.1016/j.compstruc.2006.08.015

ON SOME ASPECTS OF TORSIONAL BUCKLING OF THIN-WALLED I-BEAM COLUMNS Equation Chapter (Next) Section 1

Jacek Chróścielewski

Department of Bridge Structures,

Faculty of Civil and Environmental Engineering

Gdansk University of Technology

80-952 Gdańsk, ul. Narutowicza 11/12, Poland

Izabela Lubowiecka, Czesław Szymczak, Wojciech Witkowski**

Department of Structural Mechanics,

Faculty of Civil and Environmental Engineering

Gdansk University of Technology

80-952 Gdańsk, ul. Narutowicza 11/12, Poland

**Corresponding author

Phone: +48 58 347 21 74

Fax: +48 58 347 16 70

Email: wojwit@pg.gda.pl

ABSTRACT

The paper summarises some findings on torsional buckling of thin-walled I-beam columns. The study is divided into two parts. Firstly, the effect of initial deflection on torsional buckling load of thin-walled I-beam column is discussed. Starting from the description of kinematics, strain and stress the governing differential equations of torsional buckling are derived from the principle of stationary potential energy. The critical load of torsional buckling is determined with the aid of the perturbation approach. The numerical example concerning simply supported I-beam

column is presented and discussed on the grounds of the theory of thin-walled members and compared with the result obtained from non-linear 6-parameter theory of shells. Secondly, the localisation of local buckling modes is studied. This effect, observed during the modelling by shell theory, strongly affects the I-beam columns behaviour with relatively wide flanges.

KEYWORDS: torsional buckling, thin-walled I-beam columns, shell theory, SO(3)

1. INTRODUCTION

It is well-known [1, 2] that the bifurcation point of torsional buckling of thin-walled members of open, bisymmetric cross-section, similarly to flexural buckling, is stable and symmetric. This fact means that the small, initial geometric imperfection in the form of initial torsional angle does not cause a decrease of critical load of the torsional buckling. This is the opposite to the case of symmetric and unstable or non-symmetric bifurcation point [3, 4] where the drastic decrease of this load due to the imperfection is possible.

This paper is focused on the comparison between the results concerning torsional buckling due to flexural imperfection, obtained from thin-walled theory and two-dimensional non-linear shell model. It should be noted that similar studies have been already carried out, see for instance [5] or [6]. The latter reference is concerned with composite cantilever beams and apart from numerical analysis contains important experimental results.

The present paper is organised as follows.

Firstly, within the framework of theory of thin-walled members with open, nondeformable cross-section, an influence of initial deflection on the torsional buckling

load is investigated and analytical formulas are derived. The obtained theoretical result is valid only for linear, elastic material and for the case when the flexural buckling loads in both planes are greater than the torsional buckling load.

Secondly, a short outline of employed shell theory is provided followed by some remarks as to FEM convergence. Then the results from the above approaches are compared in pre- and post-critical range. Thirdly, we devote some attention to localisation of local buckling modes with an emphasis on issues concerning the application of compressive load. Finally, some conclusions are drawn at the end of the paper.

Sformatowano: Styl Tekst podstawowy 2 + Interlinia: Podwójne, Do lewej, Wcięcie: Z lewej: 0 cm, Interlinia: pojedyncze

Sformatowano: Do lewej

Sformatowano: Wcięcie: Z lewej: 0 cm

2. KINEMATICS OF THIN–WALLED I-BEAM COLUMN

Consider a thin-walled I-beam column axially loaded by two compressive forces P (cf. Figure 1). In the undeformed (initial, straight) configuration an arbitrary point of the member can be described by the position vector $\mathbf{r}_0$

$$\mathbf{r}_0 = x\mathbf{i} + y\mathbf{j} + z\mathbf{k} \tag{1}$$

where $\mathbf{i}$, $\mathbf{j}$, $\mathbf{k}$ are the unit vectors of x, y, z axes respectively.

Fig. 1. Compressed thin-walled I-beam column with initial imperfection

In the current configuration, after the deflection $u(x)$ in the horizontal plane x–z and after the rotation angle $\theta(z)$ of the cross-section the position vector of web points $\mathbf{R}_w$ takes the form

$$\mathbf{R}_w = u\mathbf{i} + y\cos(\theta)\mathbf{j} + y\cos(\theta)\mathbf{n} + (z+w)\mathbf{k} \tag{2}$$

where w denotes the shift of the cross-section along z–axis. In the above $\mathbf{n}$ denotes the normal vector to the deformed axis of the member, which is given by the formula

$$\mathbf{n} = \frac{\mathbf{j} \times \mathbf{R}_w'(y=0)}{\left|\mathbf{R}_w'(y=0)\right|} \tag{3}$$

with $(...)' = \frac{d(...)}{dz}$.

After some algebra the final form of position vector $\mathbf{R}_w$ becomes

$$\mathbf{R}_w = \left[u + y\frac{(1+w')\sin\theta}{\sqrt{(1+w')^2 + u'^2}} \right]\mathbf{i} + y\cos\theta\mathbf{j} + \left[z + w - y\frac{u'\sin\theta}{\sqrt{(1+w')^2 + u'^2}} \right]\mathbf{k} \tag{4}$$

The displacement vector $\mathbf{u}_w$ of the web is obtained by subtraction of equation (1) (with $x = 0$) from (4) in the form

$$\mathbf{u}_w = \mathbf{R}_w - \mathbf{r}_0 = \left[u + y\frac{(1+w')\sin\theta}{\sqrt{(1+w')^2 + u'^2}} \right]\mathbf{i} + y(\cos\theta - 1)\mathbf{j} + \left[w - y\frac{u'\sin\theta}{\sqrt{(1+w')^2 + u'^2}} \right]\mathbf{k} \tag{5}$$

The points on the middle surface of lower flange in the initial configuration are described by equation (1)~~(1)~~(1) upon setting $y = \frac{h}{2}$. In the absence of shear deformations at the flange plane, the position vector for the current configuration becomes

$$\mathbf{R}_f = u\mathbf{i} + \frac{h}{2}\cos\theta\mathbf{j} + \frac{h}{2}\cos\theta\mathbf{n} + (z+w)\mathbf{k} + \frac{\mathbf{a} \times \mathbf{R}_w'\left(y = \frac{h}{2}\right)}{\left|\mathbf{a} \times \mathbf{R}_w'\left(y = \frac{h}{2}\right)\right|}x \tag{6}$$

where

$$\mathbf{a} = \cos\theta\mathbf{j} + \sin\theta\mathbf{n} \tag{7}$$

The displacement vector $\mathbf{u}_f$ for the middle surface of flange is obtained as follows

Sformatowano: Angielski (Stany Zjednoczone)

Sformatowano: Angielski (Stany Zjednoczone)

$$\mathbf{u}_f = \mathbf{R}_f - \mathbf{r}_0\left(y = \frac{h}{2}\right) = \mathbf{r}_0 = u_f\mathbf{i} + v_f\mathbf{j} + w_f\mathbf{k} \tag{8}$$

where u_f, v_f, w_f are the components of $\mathbf{u}_f$.

The only nonzero component of Green-Lagrange strain tensor

$$E_{ij} = \frac{1}{2}\left(u_{i,j} + u_{j,i} + u_{k,i}\,u_{k,j}\right) \tag{9}$$

is

$$E_{33} = E_{zz} \equiv \varepsilon_z = \frac{\partial w_f}{\partial z} + \frac{1}{2}\left(\left(\frac{\partial u_f}{\partial z}\right)^2 + \left(\frac{\partial v_f}{\partial z}\right)^2\right) \tag{10}$$

Unfortunately, the obtained explicit formulas are too complicated for the further use. Therefore, they are expanded in power series retaining only terms of order $w' \sim u'^2 \sim h^2\theta'^2$ yielding

$$\varepsilon_z = w_f' + \frac{1}{2}u_f'^2 + u_f''\left(\frac{h}{2}\sin\theta - x\cos\theta\right) + \omega\theta'' + \frac{1}{2}r^2\theta'^2 \tag{11}$$

where $\omega = \frac{1}{2}hx$ is the sectional area of a point of the flange middle surface with given x coordinate and $r^2 = x^2 + \left(\frac{h}{2}\right)^2$ is a square of distance of that point from the member axis.

Equation (11) is valid for flanges, whereas for web the corresponding formula is obtained by setting $\frac{h}{2} \to y$ and $x = 0$ in (11).

In the presence of initial geometric imperfection given by some function $u_0(x)$ (in horizontal plane), upon the assumption of small strains, the magnitude of longitudinal strains $\bar{\varepsilon}_z$ after torsional buckling of the column is defined by the following formula

$$\bar{\varepsilon}_z = \varepsilon_z - \varepsilon_z^0 \tag{12}$$

where ε_z^0 is the initial strain being the result of initial deflection $u_0(z)$, which, based on (11), is

$$\varepsilon_z^0 = w_0' + \frac{1}{2}u_0'^2 - xu_0'' \tag{13}$$

In the above formula w_0' is the initial shortening of the member axis. Finally, for an arbitrary point of the cross-section the following equation for axial strain is obtained

$$\bar{\varepsilon}_z = \bar{w}' + \frac{1}{2}\left(u'^2 - u_0'^2\right) + u''y\sin\theta + x\left(u_0'' - u''\cos\theta\right) + \omega\theta'' + \frac{1}{2}r^2\theta'^2 \tag{14}$$

where $\bar{w} = w - w_0$ is the reduced axial displacement of the member.

3. THE GOVERNING EQUATIONS

The potential energy V_i of the column made of linear elastic material with Young modulus *E* is

$$V_i = \frac{1}{2}\int_0^l\int_A E\bar{\varepsilon}_z^2 dAdz + \frac{1}{2}\int_0^l GI_d\theta'^2 dz \tag{15}$$

where *l* is the length of the member, *A* denotes the cross-section area, *G* is the shearing modulus and I_d denotes torsion section constant. The second term in the above formula is concerned with the free torsion of the column. The work done by axial forces is

$$V_e = P\int_0^l \bar{w}' dz \tag{16}$$

Substituting (14) into (15) and performing integration over cross-section area *A* yields

$$V_i = \frac{1}{2}E\int_0^l \Big(A\bar{w}'^2 + \frac{1}{4}A\left(u'^4 - 2u'^2u_0'^2 + u_0'^4\right) + A\bar{w}'\left(u'^2 - u_0'^2\right) + u''^2 I_x \sin^2\theta + $$
$$+ I_y\left(u_0''^2 - 2u_0''u''\cos\theta + u''^2\cos^2\theta\right) + I_\omega\theta''^2 + \underline{\frac{1}{4}I_{00}\theta'^4} + I_0\bar{w}'\theta'^2 + \tag{17}$$
$$+ \frac{1}{2}I_0\theta'^2\left(u'^2 - u_0'^2\right) + GI_d\theta'^2 \Big) dz$$

where I_x, I_y, I_0 are the moments of inertia about *x* and *y* axes and polar moment of inertia respectively, I_ω is warping section constant and I_{00} stands for the second-order polar moment of inertia

$$I_{00} = \int_A r^4 dA. \tag{18}$$

Since the initial state of torsion after loss of torsional stability is of interests, the underlined term in (17) is neglected and the sine and cosine functions are expanded as $\sin\theta \approx \theta,\ \cos\theta \approx 1 - \frac{1}{2}\theta^2$.

The principle of stationary (total) potential energy $V = V_i - V_e$ with respect to the reduced axial displacement $\bar{w}$ yields

$$\bar{w}' = -\frac{1}{2}\left(u'^2 - u_0'^2\right) - \frac{1}{2}\frac{I_0}{A}\theta'^2. \tag{19}$$

Substitution of (19) into (17) and taking variations of *V* with respect to *u* and θ yields the governing set of differential equations of the problem in question

$$\begin{cases} EI_\omega\theta^{IV} + \left(P\frac{I_0}{A} - GI_d\right)\theta'' = -E\left(I_x - I_y\right)u''^2\theta - EI_y u_0''u''\theta \\ EI_y\left(u - u_0\right)^{IV} + P\left(u - u_0\right)'' = -Pu_0'' - E\left(I_x - I_y\right)u''^2\theta + \frac{1}{2}EI_y u_0''\theta^2 \end{cases} \tag{20}$$

The last two terms of right-hand side of both equations express the combination of torsional and flexural displacements and the effect of initial deflection. Neglect of these terms leads to the well-known equations of torsional buckling and of the axially compressed column with initial deflection [7].

4. APPROXIMATED SOLUTION

The solution of (20) is determined with the aid of small-parameter, which under the above assumptions, admits the following form

$$\begin{cases} \theta(z) = \varepsilon\theta_1(z) + \varepsilon^2\theta_2(z) + \ldots \\ u(z) = u_1(z) + \varepsilon u_2(z) + \ldots \\ P = P_0 + \varepsilon P_1 + \ldots \end{cases} \tag{21}$$

with ε as the small parameter.

A zero-order approximation leads to

$$EI_y\left(u-u_0\right)^{IV} + P\left(u-u_0\right)'' = -Pu_0'' \tag{22}$$

whereas the first-order to

$$EI_\omega\theta_1^{IV} + \left(P_0\frac{I_0}{A} - GI_d\right)\theta_1'' = -E\left(I_x - I_y\right)u_1''^2\theta_1 - EI_y u_0'' u_1''\theta_1 \tag{23}$$

Assuming that the critical load of torsional buckling P_{cr}^{θ} is smaller than flexural critical load about *y* axis – P_{cr}^{y}, it is possible to find the solution of (22) for a given shape of initial deflection $u_0(z)$ and the substitute it to (23).

For a simply supported member with initial deflection

$$u_0(z) = U_0\sin\frac{\pi z}{l} \tag{24}$$

this yields

$$u_1(z) = U_0\frac{1}{1-\dfrac{P_0}{P_{cr}^y}}\sin\frac{\pi z}{l} \tag{25}$$

Substitution of (25) into (23) yields linear differential equation with variable coefficients

$$EI_\omega \theta_1^{IV} + \left(P_0 \frac{I_0}{A} - GI_d \right) \theta_1'' + \left(\frac{\pi}{l} \right)^4 EU_0^2 \sin^2 \frac{\pi z}{l} \left(\frac{I_x - I_y}{\left(1 - \frac{P_0}{P_{cr}^y} \right)^2} + \frac{I_y}{1 - \frac{P_0}{P_{cr}^y}} \right) \theta_1 = 0 \,. \quad (26)$$

The above equation is solved in an approximated manner with the aid of Galerkin method for the first approximation given by

$$\theta_1(z) = \bar{\theta}_1 \sin \frac{\pi z}{l}. \quad (27)$$

Substitution of (27) into (26), multiplication by $\sin \frac{\pi z}{l}$ and integration over member length yields the formula

$$EI_\omega \left(\frac{\pi}{l} \right)^2 - \left(P_0 \frac{I_0}{A} - GI_d \right) + \frac{3}{4} \left(\frac{\pi}{l} \right)^2 EU_0^2 \left(\frac{I_x - I_y}{\left(1 - \frac{P_0}{P_{cr}^y} \right)^2} + \frac{I_y}{1 - \frac{P_0}{P_{cr}^y}} \right) = 0, \quad (28)$$

which gives the estimation of the critical load of torsional buckling $P_{cr}^\theta \cong P_0$. The above nonlinear equation was solved using the bisection method.

It is worth ~~of~~ emphasising that the above reasoning may be easily repeated for initial imperfection perpendicular to the *x* axis which is the major axis of cross section. In this case the imperfection is given by

$$v_0(z) = V_0 \sin \frac{\pi z}{l} \quad (29)$$

which gives the counterpart of equation (28) in the form

$$EI_\omega \left(\frac{\pi}{l} \right)^2 - \left(P_0 \frac{I_0}{A} - GI_d \right) + \frac{3}{4} \left(\frac{\pi}{l} \right)^2 EV_0^2 \left(\frac{I_y - I_x}{\left(1 - \frac{P_0}{P_{cr}^x} \right)^2} + \frac{I_y}{1 - \frac{P_0}{P_{cr}^x}} \right) = 0. \quad (30)$$

As it has been already mentioned, formulas (28) and (30) make sense only if flexural buckling loads are greater than torsional buckling load. These loads, for the simply supported member in question, may be easily obtained from the well-known formulas

$$P_{cr}^{x} = \frac{\pi^2 EI_x}{l^2}, \quad P_{cr}^{y} = \frac{\pi^2 EI_y}{l^2}$$
$$P_0 = \frac{A}{I_0}\left(\frac{\pi^2 EI_\omega}{l^2} + GI_d \right) \tag{31}$$

Given these equations, we have examined the variations of critical loads on the flange width. Figure 2 depicts the results for data given in Fig. 1.

Fig. 2. Variations of critical loads vs flange width *B*

In this study we focused our attention to two flange widths 0.2 and 0.4*m*. As indicated in Fig. 2 in the latter case, the torsional buckling load is the smallest while in the former this is not a case. This may be alleviated by imposing a vertical imperfection v_0, initiating thus flexural buckling in the direction perpendicular to *x* axis where we have $P_{cr}^{x} > P_0$ which solves the problem. Therefore, in the following calculations we assumed vertical imperfection v_0 in form given by equation (29).

Bearing in mind, however, the approximate character of the above formulas, the analytical results are deferred to the following section where the evaluated critical load is compared with that from nonlinear shell theory.

5. OUTLINE OF SHELL THEORY

In the finite element method (FEM) analysis of thin-walled members, several approaches may be distinguished. For instance, one may develop an element from expressions for the first and second variation of the total energy of the member. This approach has been used, among others, in [8], [9] or [10] leading to elements with seven degrees of freedom per node.

In this paper we use another possibility. We treat the thin-walled member as an assembly of shell panels modelled by shell finite elements. The fundamentals of the shell theory employed here may be found, for instance, in [11]~~[11]~~[6] while numerical implementation has been discussed, for example, in [12]~~[12]~~[7], [13]~~[13]~~[8] ~~[9]~~ and [14]. In general, the motion of the irregular shell structure (like, for instance, I-beam column) can be described by the displacement vector field $\boldsymbol{u}(\boldsymbol{x})=\boldsymbol{y}(\boldsymbol{x})-\boldsymbol{x}$, where $\boldsymbol{x}\in M$ and $\boldsymbol{y}(\boldsymbol{x})$ are position vectors of the undeformed and deformed shell base surface, respectively, together with the independent proper orthogonal tensor field $\boldsymbol{Q}(\boldsymbol{x})$ representing the mean rotary motion of the shell ~~cross sections~~fibres i.e. $\boldsymbol{t}_i=\boldsymbol{Q}\boldsymbol{t}_i^0$, $i=1,2,3$ – see Figure 3. The fields $\boldsymbol{y}(\boldsymbol{x})$ and $\boldsymbol{Q}(\boldsymbol{x})$ are assumed to be continuous during the motion, and on any stationary singular curve $\Gamma\subset M$ determining an irregularity (fold, intersection, branching, etc.) i.e. $\boldsymbol{y}_\Gamma(\boldsymbol{x}_\Gamma)=\boldsymbol{y}(\boldsymbol{x})|_\Gamma$, $\boldsymbol{Q}_\Gamma(\boldsymbol{x}_\Gamma)=\boldsymbol{Q}(\boldsymbol{x})|_\Gamma$.

We confine our considerations to hyper-elastic shells for which there exists a 2D strain energy density $W(\boldsymbol{\varepsilon}_\beta,\boldsymbol{\kappa}_\beta;\boldsymbol{x})$ of the shell strain vectors $\boldsymbol{\varepsilon}_\beta=\boldsymbol{y}_{,\beta}-\boldsymbol{Q}\boldsymbol{x}_{,\beta}$ and $\boldsymbol{\kappa}_\beta=\mathrm{ad}^{-1}(\boldsymbol{Q}_{,\beta}\boldsymbol{Q}^{\mathrm{T}})$. Then the constitutive relations of the shell material are given by $\boldsymbol{n}^\beta=\partial W/\partial\boldsymbol{\varepsilon}_\beta$, $\boldsymbol{m}^\beta=\partial W/\partial\boldsymbol{\kappa}_\beta$, where $\boldsymbol{n}^\beta(\boldsymbol{x})$ and $\boldsymbol{m}^\beta(\boldsymbol{x})$ are the internal stress and couple resultant vectors, respectively.

Sformatowano: Styl Tekst podstawowy 2 + Interlinia: Podwójne, Interlinia: pojedyncze

When expressed in the weak form, the initial-boundary value problem for the branched shell-like structure can be formulated as follows. Given the external resultant force and couple vector fields $\boldsymbol{f}(\boldsymbol{x})$ and $\boldsymbol{c}(\boldsymbol{x})$ on $\boldsymbol{x} \in M \setminus \Gamma$, $\boldsymbol{n}^*(\boldsymbol{x})$ and $\boldsymbol{m}^*(\boldsymbol{x})$ along ∂M_f, $\boldsymbol{f}_\Gamma(\boldsymbol{x}_\Gamma)$ and $\boldsymbol{c}_\Gamma(\boldsymbol{x}_\Gamma)$ along the singular curve $\Gamma \subset M$, find a curve $\mathsf{u}(\boldsymbol{x}) = (\boldsymbol{u}(\boldsymbol{x}), \boldsymbol{Q}(\boldsymbol{x}))$ on the configuration space $C(M, E^3 \times SO(3))$ such that for any continuous kinematically admissible virtual vector field $\mathsf{w}(\boldsymbol{x}) \equiv (\boldsymbol{v}(\boldsymbol{x}), \boldsymbol{w}(\boldsymbol{x}))$ the following principle of virtual work is satisfied:

$$G[\mathsf{u};\mathsf{w}] = \iint_{M\setminus\Gamma} [\boldsymbol{n}^\beta \cdot (\boldsymbol{v}_{,\beta} + \boldsymbol{y}_{,\beta} \times \boldsymbol{w}) + \boldsymbol{m}^\beta \cdot \boldsymbol{w}_{,\beta}]\, da - \iint_{M\setminus\Gamma} (\boldsymbol{f} \cdot \boldsymbol{v} + \boldsymbol{c} \cdot \boldsymbol{w})\, da$$
$$- \int_{\partial M_f} (\boldsymbol{n}^* \cdot \boldsymbol{v} + \boldsymbol{m}^* \cdot \boldsymbol{w})\, ds - \int_\Gamma (\boldsymbol{f}_\Gamma \cdot \boldsymbol{v}_\Gamma + \boldsymbol{c}_\Gamma \cdot \boldsymbol{w}_\Gamma)\, ds = 0. \tag{32}$$

In (32) it is implicitly assumed that the kinematic boundary conditions $\boldsymbol{u}(\boldsymbol{x}) = \boldsymbol{u}^*(\boldsymbol{x})$ and $\boldsymbol{Q}(\boldsymbol{x}) = \boldsymbol{Q}^*(\boldsymbol{x})$ are satisfied along the complementary part $\partial M_d = \partial M \setminus \partial M_f$ of the shell boundary, and the virtual vector fields are kinematically admissible if $\boldsymbol{v}(\boldsymbol{x}) = \boldsymbol{0}$ and $\boldsymbol{w}(\boldsymbol{x}) = \boldsymbol{0}$ along ∂M_d. Approximated spatially by finite element method, equation (32) is solved using Newton method. However, due to the presence of rotation group $SO(3)$, the configuration space is not a linear. Therefore, special techniques are required for interpolation, linearisation and iteration. For more details see [12][~~12~~][7], [13][~~13~~][8] ~~an d~~ [9]~~or~~ [14].

It should be stressed that in this theory, ~~-~~the sixth DOF (the so-called drilling degree-of-freedom) enters the theory in the natural way. Therefore, without resorting to any special techniques or additional assumptions, all elements have six engineering degrees of freedom at each node – see Figure 3. This property is crucial in the analysis of irregular shell-like structures such as those with branches or intersections, which makes these elements a powerful, reliable and well-suited tool for analysis of thin-walled members.

Within this framework, an own computer code (called CAM) was developed with, among others, 4–, 9– and 16–node displacement-rotation based C^0 elements. These elements, denoted by CAMe4, CAMe9 and CAMe16 respectively are used here for computations.

Fig. 3. Typical finite element with 6 degrees of freedom on the reference surface

6. NUMERICAL EXAMPLES

6.1. Critical load of torsional buckling

Consider an axially compressed, simply supported I-beam column as depicted in Fig. 1 with flange width $B = 0.2\text{m}$. Following [1], [7] ~~[1, 5]~~, for an ideal I-beam column, the torsional buckling load is, according to equation (31)~~(31)(31)~~$_2$, 3.34 MN. In FEM analysis, due to bisymmetry of the column cross-section and ~~anti-~~symmetry of the buckling mode, only a ~~quarter~~ half of the column was discretised with boundary conditions depicted in Fig. 4. In the non-linear stability analysis, the one-parameter dead-load of form $P = \lambda P_{ref}$ (where $P_{ref} = q_{ref} A = 1\text{MN}$ is uniformly distributed over cross-section) is used. As the imperfection load, the torque $M_{impf} = 100\,\text{Nm}$ is applied at the longitudinal axis – see Fig. 4. The equilibrium path of the column with imperfection is traced using load control and arc-length control techniques until reaching neighbourhood of the primary path. Then, the imperfection load is removed yielding jump on the primary path. Next, by using the displacement control technique until control displacement u at point j (denoted $u_{(j)}$), is close to zero, the beam is restored to its symmetric configuration at the bifurcation point yielding critical torsional load multiplier λ_{CR}. ~~In order to enforce the torsional buckling all nodes at the longitudinal~~

Sformatowano: Do lewej, Wcięcie: Z lewej: 0 cm, Pierwszy wiersz: 1,27 cm

Sformatowano: Wcięcie: Pierwszy wiersz: 1,27 cm

Sformatowano: Angielski (Stany Zjednoczone)

Sformatowano: Angielski (Stany Zjednoczone)

~~axis have *u* and *v* displacement constrained.~~ The above described technique of finding critical load is depicted in Fig. 5.

Fig. 4. Torsional stability of I-beam column, FEM discretisation and loads

Fig. 5. Equilibrium paths: primary + imperfection and ideal

In Table 1 some of the numerical results obtained are presented. For the comparison and verification the Table contains the result obtained with the help of Enhanced Assumed Strain element EAS14m1, described in [14]~~[14]~~[10]. The discretisations, denoted by (lower flange+web+upper flange)×length, are given for whole beam while the number of degrees of freedom is computed for one quarter of the beam taken into consideration in FEM calculations. All values in Table 1 were obtained with full integration (FI) of element's matrices. These values are depicted in Figure 6.

Fig. 6. Convergence analysis

As it may be noted CAMe4 elements (filled diamonds) with full integration (FI) overestimate values of critical load multiplier and the convergence rate is rather poor. This is attributed to the locking phenomenon~~a~~ well known from application of low–order Lagrange-type elements. In order to alleviate this flaw a reduced integration technique may be applied at the expense of, however, the so-called spurious zero-energy modes which may pollute or even completely destroy the solution. These facts ruled out CAMe4 elements. Table 1 indicates that other elements exhibit faster convergence with good accuracy. A deeper inspection into the results, carried out in ~~[9]~~ [12], indicated supremacy of CAMe16 elements over CAMe9 in terms of locking and spurious modes.

Therefore, for the further research CAMe16 elements in (2+2+2)×20 mesh are used which is distinguished by boldface character in Table 1. Figure 5 depicts the obtained load-deformation path with the obtained critical load multiplier $\lambda_{CR} = 3.329$. This result is confirmed by the value $\lambda_{CR} = 3.321$ obtained with the help of EAS14m1 element.

In Fig. 5 one configuration in the pre-buckling configuration is selected for $\lambda = 3.288$ in order to throw some light on the deformed geometry. Figure 7 ~~reproduces~~ depicts ten-times magnified deformation corresponding to $\lambda = 3.288$. Here $-u_j \approx 1.058\,cm$.

Fig. 7. Ten-times scaled deformation at $\lambda = 3.288$ (pre-buckling configuration)

Note that the longitudinal axis remains straight ~~which is~~ due to the imposed boundary conditions. In addition, the edge distinguished by the dashed line is in the form of a single wave. In the well-advanced post-critical configuration, however, as it will be shown latter, this will be not a case.

6.2. Influence of initial imperfection on torsional buckling load

Sformatowano: Czcionka: Pogrubienie

Sformatowano: Wcięcie: Pierwszy wiersz: 0 cm

With ~~this preliminary facts~~these preliminary facts we are ready to investigate the influence of the initial deflection v_0 on the critical load of torsional buckling. Figure 8 depicts the comparison between analytical results from equation (30) and those from nonlinear theory of shells for the column with flange width $B = 0.2m$. Here due to symmetry of the imperfection v_0, FEM calculations were carried out for ½ beam.

Fig. 8. Influence of initial imperfection v_0 on critical load: analytical and FEM results

In FEM calculations, five values of amplitudes of the initial deflection v_0 (applied as shown in Figure 4 in the middle of the beam) are considered. As it may be observed, the imposed flexural imperfection causes a drastic decrease of the torsional buckling load. Note also very good agreement between the analytical and numerical results. The FEM results slightly underestimate the values, which is due to the initial differences in assessment of the critical load $P_{CR}(v_0 = 0)$ value (cf. Tab. 1).

Associated with the decrease of critical load due to initial imperfection v_0 is the increase of total deflection i.e. critical deflection v_{CR} corresponding to the instant of loss of stability. Figure 9 depicts the variations of v_{CR} due to the imposed imperfection v_0. ~~The grey dashed line with open diamonds corresponds to classical thin-walled beam theory while solid line represents the FEM results.~~

Fig. 9. Effect of initial imperfection v_0 on critical deflection v_{CR}: analytical and FEM results

As it ~~is~~ may be observed~~seen~~, the above results are in good agreement. Starting with zero imperfection (vertical axis) we arrive precisely at the critical load multiplier $\lambda_{CR} = 3.329$ in FEM case or $\lambda_{CR} = 3.343$ in analytical case. Then, with the growth of the imposed imperfection we note the decrease of critical load with simultaneous growth of critical deflection v_{CR}. The points on the upper end of each branch mark the computed critical deflection v_{CR}. These values are connected by the thin dashed line in order to portrait the trend of the phenomenon. For instance, for $v_0 = 0.5\,cm$ the critical deflection v_{CR} is found to be 1.04 cm (which gives $1.04 - 0.5 = 0.54\,cm$ increment)

whereas in case of $v_0 = 5.0\,cm$ the computed v_{CR} is $9.16\,cm$ ($9.16 - 5.0 = 4.16\,cm$ increment).

In order to give some idea about the influence of v_0 on total deflections, in Fig. 10 displacements of the right (R) and left (L) edge of the bottom flange along the column axis are depicted. Due to symmetry only half of the beam is shown.

Fig. 10. Deformation of the lower flange (FEM): edge displacements along z-axis

The "snap-shot" of the deformed lower flange was taken in the pre-buckling state. In connection with Fig. 7 and Fig. 10 it is seen that the edges deform~~,~~ taking the shape of single wave. It has been mentioned, however, that in well-advanced post-critical state this is no longer a case. In order to throw some light on that issue, and to address the post-critical analysis, in Fig. 11 a comparison of load-deformation paths from analytical and FEM studies is presented.

Fig. 11. Post-critical equilibrium paths after torsional buckling

As expected, the obtained bifurcation point is stable and symmetric. Note also that analytical formula gives reasonable approximation for $\theta < 1$. Above this threshold, the discrepancies between the results attain unacceptable values leading to the conclusion that more terms should be added in order to ensure better accuracy of analytical solution at this range of post-critical analysis.

To picture the deformation shape at this stage of analysis~~, one configuration is chosen in Fig. 11. The deformed not scaled mesh is depicted~~ some representative configurations are shown in Fig. 12.

Fig. 12. Deformed beam in post-critical range

For $\lambda = 6.135$, the angle of torsion of the middle cross-section is, according to Fig.~~10~~11~~,~~ around 2 radians. The edges of lower and upper flange take complicated forms and we may note some local modes of instability of the flanges. For the ~~sake of~~ comparison~~,~~ in Fig. 12 another configuration for $\lambda = 11.25$ is included ~~in Fig. 12 ,~~ which has not its representation in Fig. 11. At this stage the shape of flanges is even more complicated and the local forms are clearly pronounced with local collapse of flanges and changes of curvature.

6.3. Effect of change of flange width on critical load

Further analysis deals with the influence of flange width for on the torsional buckling load. The widths are taken from range $B = (0.15 \div 0.34)m$. For given value of width and for variable initial deflection amplitude the buckling load is computed using (30). The results are depicted in Fig. 13.

Fig. 13. Critical load vs initial imperfection for different flange widths

Figure 13 brings up interesting observation namely~~,~~ for some values of flange width, the initial imperfection causes the decrease of critical load which is consistent with the trend from Fig 9. There is however a threshold above which the critical load grows with the increase of imperfection. This may be attributed to the paradox of torsional buckling – see, for example, [15]~~[15]~~[11], [16]~~[16]~~[12]~~. or .~~

6.4. Localisation of the local buckling mode

Sformatowano: Czcionka: Pogrubienie

Sformatowano: Wcięcie: Pierwszy wiersz: 0 cm

We now turn our attention to the problem of localisation of the local mode of buckling. Consider an I-beam column as in Figure 14 with $B = 0.4m$, discretised as in previous section i.e. CAMe16 (4+4+4)×40 elements for whole beam. In this case, torsional buckling load according to $(31)_2$ is 8.54 MN. Suppose that for $z = 0.5L$ there is a segment of length $c = L/20 (= 20cm)$ (two rows of elements) which has reduced thickness of upper and lower flanges as shown in Fig. 14. Let us define parameter $\delta = \frac{t_{red}}{t}$ describing ratio of reduced thickness. Exploiting the fact that the column has three symmetry planes, the calculations in this part of the study are carried out for $1/8$ of the beam.

Fig. 14. I-beam column with notch – buckling mode localisation

Two different compressive loads were considered, namely: uniformly distributed load (as ~~in~~in the previous sections) and two point forces applied at the intersection of the web with flanges. Fig. 15 and Fig. 16 depict post-critical equilibrium paths.

Fig. 15. Buckling mode localisation – equilibrium path for uniformly distributed load

Fig. 16. Buckling mode localisation – equilibrium path for concentrated load

On examining Fig. 15 and 16 we may note that way in which load is applied has significant influence on qualitative and quantitative character of results. While in case

of concentrated loads the computed vertical displacement of flanges are of the same sign and equilibrium paths share the same shape, for uniformly distributed load two cases of δ have different signs than remaining results. ~~This discrepancies~~These discrepancies are even more pronounced if we examine deformation of the flange. Fig. 17 and 18 show vertical displacement of the flange edge along column length.

Fig. 17. Buckling mode localisation – vertical displacement of flange edge for uniformly distributed load

Fig. 18. Buckling mode localisation – vertical displacement of flange edge for concentrated load

Bold line in Fig. 17 and 18 corresponds to $\delta = 1$ case i.e. without thickness reduction. Clearly, the deformations in both cases under consideration are different. In the first case – uniformly distributed load - there may be observed a phase lag for $\delta = 0.91$ and $\delta = 0.94$ with simultaneous change of sign, which corresponds exactly to Fig. 15. The amplitudes for $\delta = 1$ decrease as z approaches $L/2$ while for reduced thickness they have tendency to grow. In case of concentrated load the obtained shapes have the same qualitative character with growing amplitudes as $z \to L/2$. Here, for $\delta = 1.00$, the amplitude is constant along the beam.

In order to summarise the results let us define two coefficients The first is the amplitude coefficient $\alpha = \frac{|\bar{v}_{\max}|}{|\bar{v}_{\min}|}$ which describes ratio of maximal computed vertical displacement $\bar{v}_{\max}$ over minimal amplitude of deformation wave along flange edge $\bar{v}_{\min}$

for given thickness reduction δ. The second coefficient is $\alpha_0 = \alpha(\delta = 1)$. Figure 19 shows ratio α / α_0 versus δ with the latter value expressed in %.

Fig. 19. Buckling mode localisation – ratio of amplitudes of the local buckling α / α_0 vs thickness reduction δ coefficient

The results from this section indicate in conjunction with analytical value of torsional buckling load i.e. 8.54 MN (31), that local buckling of flange occurs before torsional buckling. This observation is independent of kind of applied load. For example, if uniformly distributed load is applied with $\delta = 0.99$, the buckling occurs at c.a. 5.9 MN. What we deal with here, therefore, is compound buckling triggered by local instability on flange part.

CONCLUSIONS

The torsional buckling phenomenon of thin-walled I-beam columns was studied. Two different approaches: one-dimensional column and the six-parameter non-linear shell model are investigated. An effect of initial curvature of axis of the column on torsional load has been studied. The obtained results show the decrease of critical load with the increase of initial imperfection. In addition, the critical deflection has been evaluated. Both models are in very good agreement. Post-critical analysis shows that one-dimensional model, to some extent, gives acceptable results. In well-advanced range of displacements however, the discrepancies between two models grow indicating that some modifications of the one dimensional model are necessary.

Some differences are noticed in case of the I-beam columns with relatively wide width. This fact enables us to formulate two main conclusions.

Firstly, the FEM model reveals sensitivity to the way at which the external load is applied. It follows from the FEM discretisation of the shell I-column since the load, as all of the FEM functions, must be defined in nodes of the mesh. It gives the rise to the question how to find an appropriate equivalence between concentrated load from one-dimensional model and load in FEM setting. In the light of the above study the results may differ qualitatively and quantitatively.

Secondly, some local effects on the buckling modes are observed. While for columns with narrow flanges the loss of stability occurs in global way, the local effects have considerable influence on stability of columns with wide flanges. Therefore, in the former case the analytical and FEM solutions agree while in the latter one should expect some discrepancies. These facts indicate that behaviour of beams with wide flanges should be understood as a shell rather than rod structure. This observation has valuable meaning in the design of compressed elements in which the local buckling plays the crucial role. In particular, in the light of the findings form the last section, a conclusion may be drawn that in case of wide flanges the assumption as to nondeformable cross-section in not satisfied.

ACKNOWLEDGEMENTS

This work has been supported by Polish State Committee under grant KBN 5 T07A 00825.

Wojciech Witkowski is awarded by Foundation for Polish Science.

REFERENCES

[1] Szymczak C. Buckling and initial post-buckling behaviour of thin-walled I column. ~~Int. J. Co~~mputers and ~~Structures~~ Structures 1980; 11(6): 481–487.

[2] Pedersen C. Stability properties and non-linear behaviour of thin-walled elastic beams of open cross-section. Department of Structural Engineering, Technical University of Denmark, Serie R, No 149, 1982.

[3] Thompson J.M.T., Hunt G.W. A general theory of elastic stability. London: John Wiley and Sons, 1973.

[4] Huseyn K. Nonlinear theory of elastic stability. Leyden Noordhoff International Publishing, 1975.

[5] Usuki S, Hasebe K. Effects of pre-buckling deflections on local, distortional and lateral-torsional buckling of I-beams. Proceedings of Japan Society of Civil Engineers, Structural Engineering/Earthquake Engineering. 1985; 2(2): 221-224.

[6] Qiao P, Zou G, Davalos JF. Flexural–torsional buckling of fiber-reinforced plastic composite cantilever I-beams. Composite Structures 2003; 60: 205–217.

~~[5]~~[7] Timoshenko S.P., Gere J.M. Theory of elastic stability. New York: Mc Graw-Hill, 1961, II ed.

[8] Ronagh HR, Bradford MA. Non-linear analysis of thin-walled members of open cross-section. International Journal for Numerical Methods in Engineering 1999; 46: 535-552.

[9] Pi YL, Bradford MA. Effects of approximations in analyses of beams of open thin-walled cross-section-part I: Flexural-torsional stability. International Journal for Numerical Methods in Engineering 2001; 51:757-772.

[10] Pi YL, Bradford MA. Effects of approximations in analyses of beams of open thin-walled cross-section-part II: 3-D non-linear behaviour. International Journal for Numerical Methods in Engineering 2001; 51:773-790

Sformatowane: Punktory i numeracja

~~[6]~~[11] Libai A., Simmonds J.G. Nonlinear elastic shell theory. In: Advances in Applied Mechanics 23, 271-371, New York: Academic Press, 1983

~~[7]~~[12] Chróscielewski J., Makowski J., Stumpf H. Genuinely resultant shell finite elements accounting for geometric and material non-linearity. International Journal for Numerical Methods in Engineering~~Int. J. Numer. Methods Engng.~~ 1992; 35: 63-94.

~~[8]~~[13] Chróścielewski J., Makowski J., Stumpf H. Finite element analysis of smooth, folded and multi-shell structures. Computer~~,~~ Methods in~~,~~ Applied~~,~~ Mechanics and ~~,~~ Engineering~~ng.~~ 1997; 141: 1-46.

~~[9] Chróscielewski J.: Family of C^0 finite elements in six parameter nonlinear theory of shells. Gdańsk University of Technology Publishers, Civil Eng Series, 540(LIII), Gdańsk, Poland 1996.~~

[14] ~~Witkowski W., Chróścielewski J.: Enhanced assumed strain 4-node element in 6-field nonlinear shell theory, In: Garstecki, Mochnacki, Szczygiol, editors. Proceedings of 16th International Conference CMM 2005 – *Computer Methods in Mechanics*, Częstochowa, Poland, June 21-24, 2005~~ Chróścielewski J, Witkowski W. 4-node semi-EAS element in 6–field nonlinear theory of shells. International Journal for Numerical Methods in Engineering, in press~~,~~

~~[11]~~[15] Cywiński Z. and Kollbrunner C.F., Drillknicken dünnwandiger I-Stäbe mit veränderlichen, doppelt symmetrischen Querschnitten. *Inst. for Engrg. Res.*, Zurich, Switzerland, **18**, 1971 pp.1-35 (in German).

~~[12]~~[16] Szymczak C.~~,~~ Chróścielewski J.~~,~~ Lubowiecka I.~~,~~ On the paradox of torsional buckling of thin-walled I columns. Archive of Civil Engineering 2003; XLIX:~~ 2003,~~ 3-13.

Sformatowano: Angielski (Stany Zjednoczone)

Sformatowano: Normalny, Interlinia: Podwójne, Numerowanie + Poziom: 1 + Styl numeracji: 1, 2, 3, … + Rozpocznij od: 1 + Wyrównanie: Na lewo + Wyrównanie: 0 cm + Tabulator po: 0,4 cm + Wcięcie: 0,4 cm, Nie dopasowuj odstępu między łacińskim i azjatyckim tekstem, Nie dopasowuj odstępu między azjatyckim tekstem i liczbami, Tabulatory: 0,63 cm, Do lewej

Sformatowano: Angielski (Stany Zjednoczone)

Sformatowano: Angielski (Stany Zjednoczone)

Sformatowano: Angielski (Stany Zjednoczone)

Sformatowano: Niemiecki (Niemcy)

Sformatowano: Polski

Sformatowano: Polski

~~[13]~~[17] H. Chen, Liu F., Hsiao K. Co-rotational finite element formulation for doubly symmetric thin-walled beams with variable open section. In: Garstecki, Mochnacki, Szczygioł, editors. Proceedings of 16th International Conference CMM-2005 – Computer Methods in Mechanics, Częstochowa, Poland, June 21-24, 2005.

Sformatowano: Czcionka: Nie Kursywa

ON SOME ASPECTS OF TORSIONAL BUCKLING OF THIN-WALLED I-BEAM COLUMNS

Jacek Chróścielewski
Department of Bridge Structures,
Faculty of Civil Engineering
Gdańsk University of Technology

Izabela Lubowiecka, Czesław Szymczak, Wojciech Witkowski**
Department of Structural Mechanics,
Faculty of Civil Engineering
Gdańsk University of Technology

**Corresponding author
Phone: +48 58 347 21 74
Fax: +48 58 347 16 70
Email: wojwit@pg.gda.pl

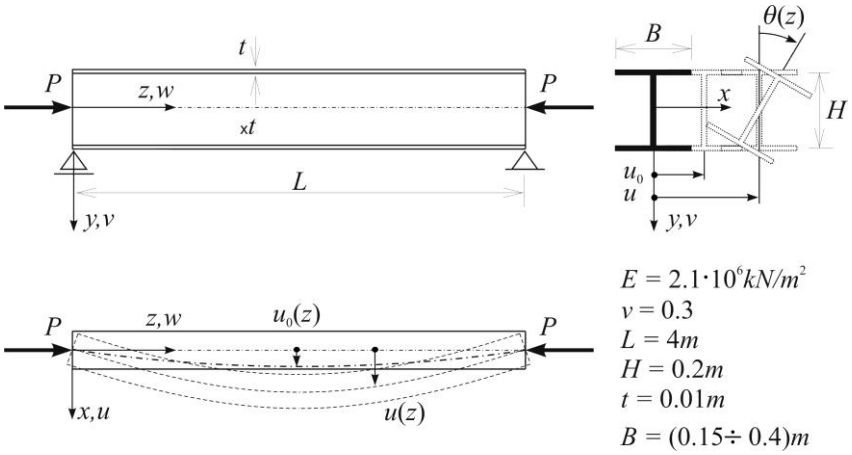

Fig. 1. Compressed thin-walled I-column with initial imperfection

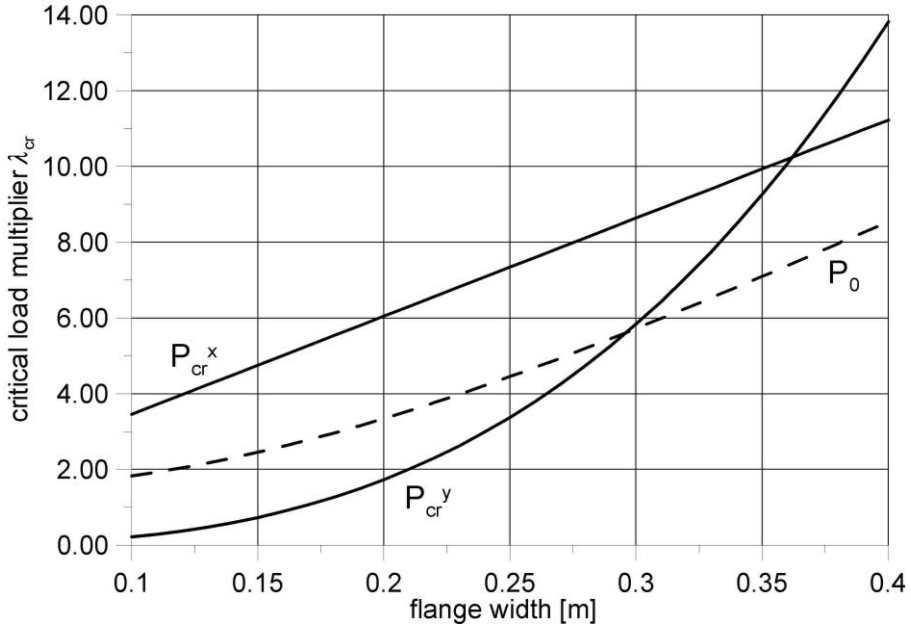

Fig. 2. Variations of critical loads on flange width *B*

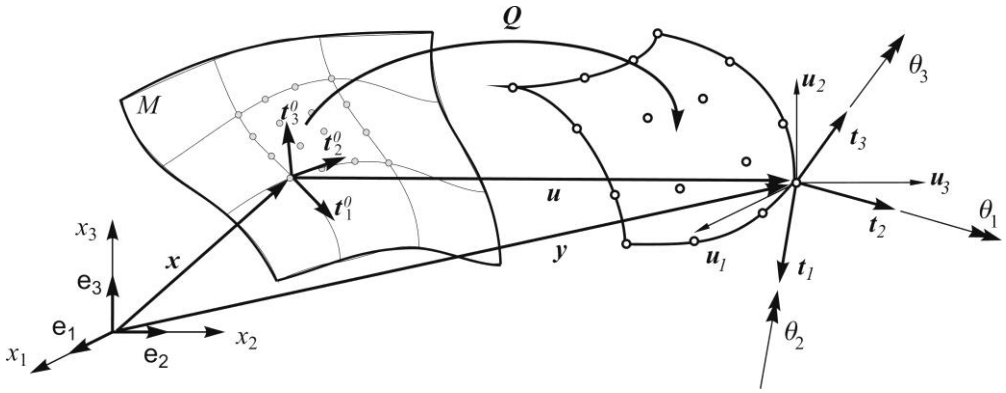

Fig. 3. Typical finite element with 6 degrees of freedom on the reference surface *M*

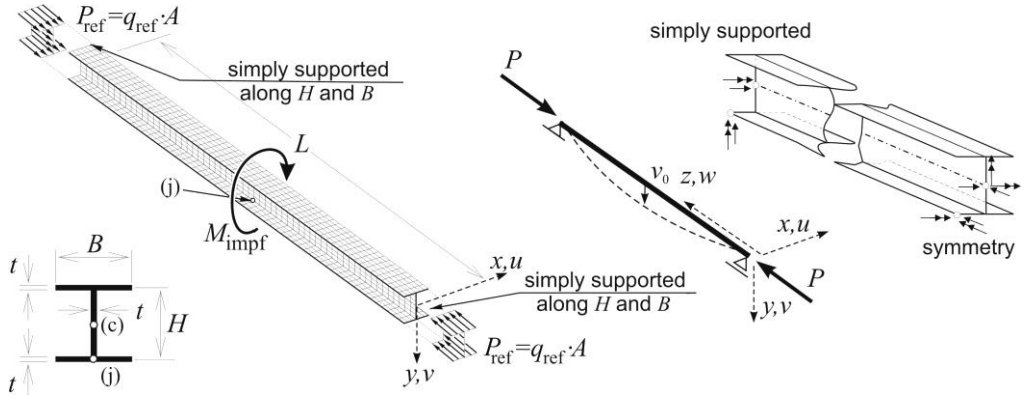

Fig. 4. Torsional stability of I-beam, FEM discretisation, load and boundary conditions

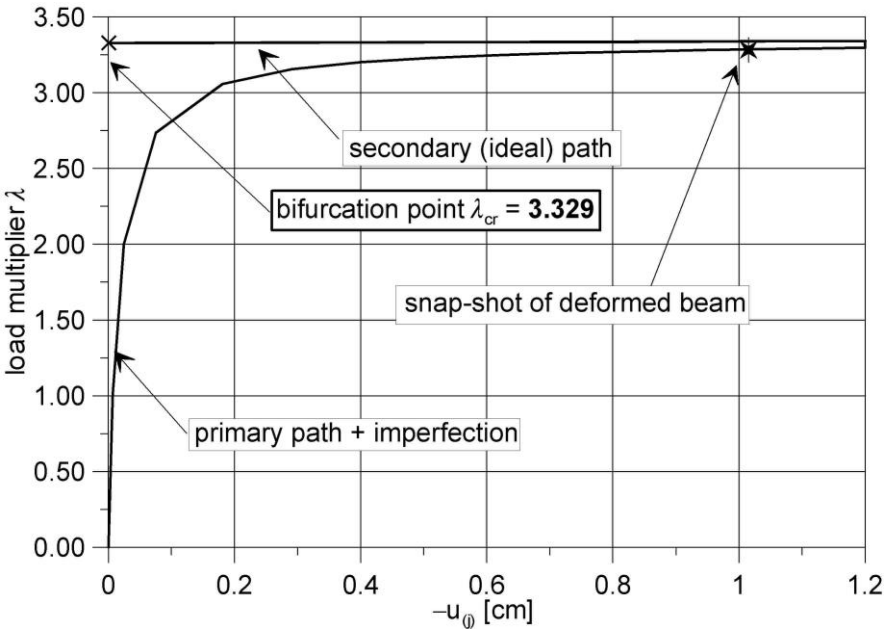

Fig. 5. Equilibrium paths: primary + imperfection and ideal

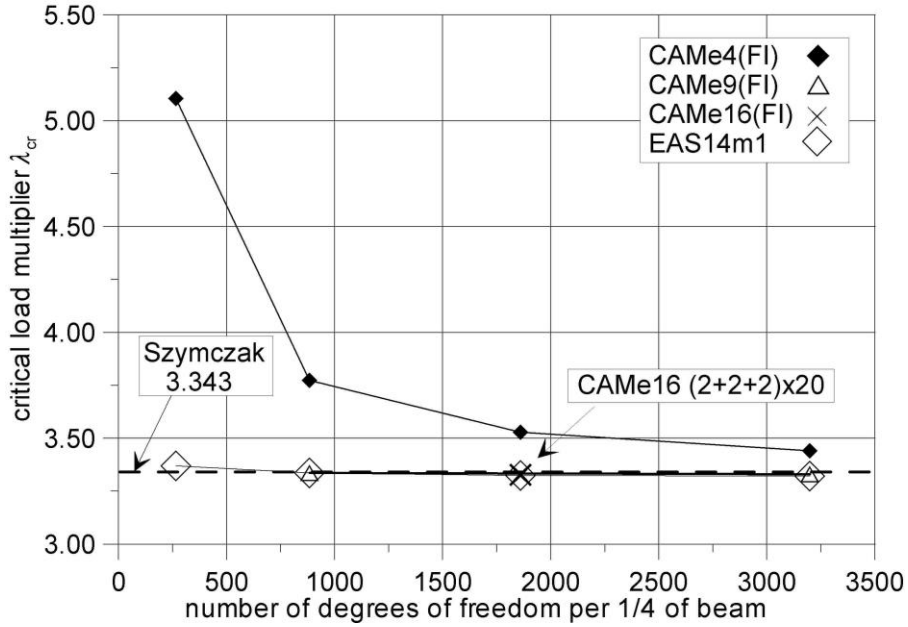

Fig. 6. Convergence analysis

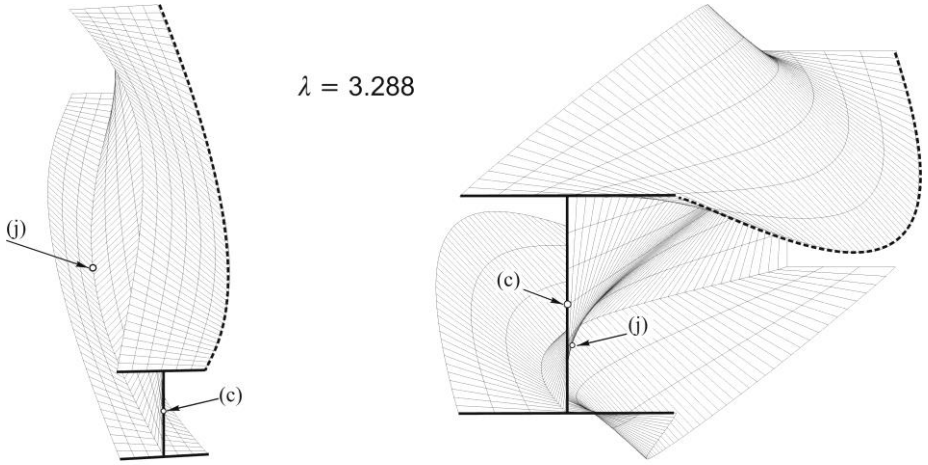

Fig. 7. Ten-times scaled deformation at $\lambda = 3.288$ (pre-buckling configuration)

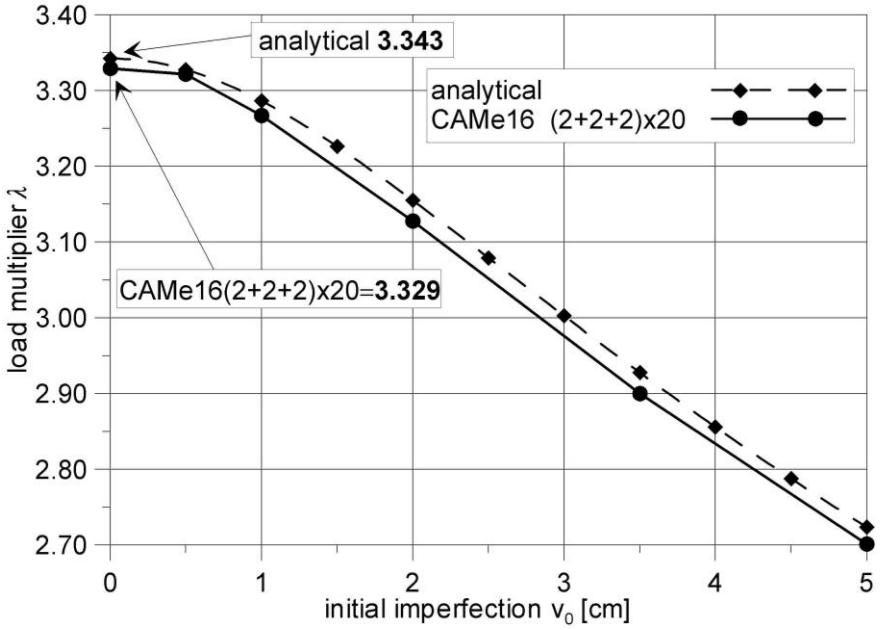

Fig. 8. Influence of initial imperfection v_0 on critical load: analytical and FEM results

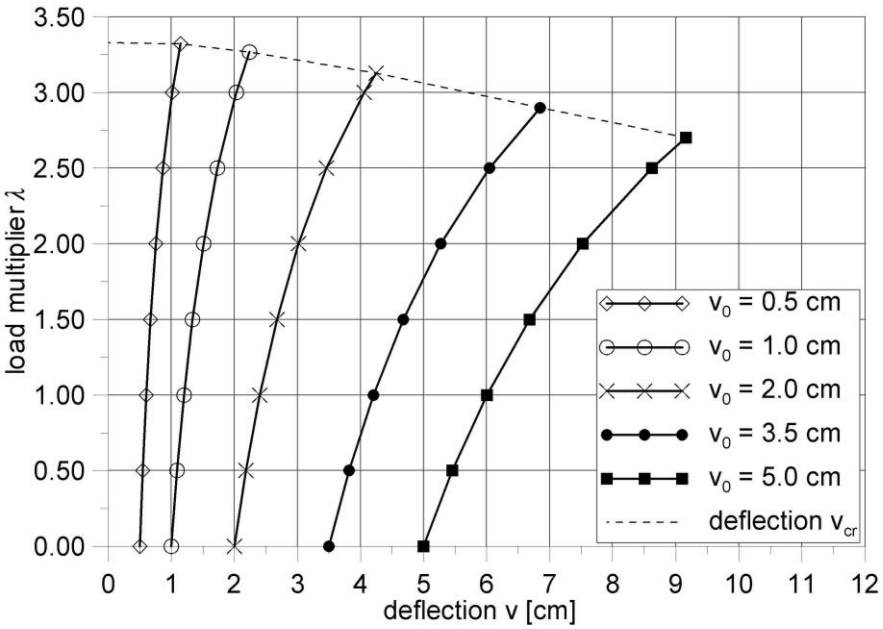

Fig. 9. Influence of initial imperfection v_0 on critical deflection v_{CR}: analytical and FEM results

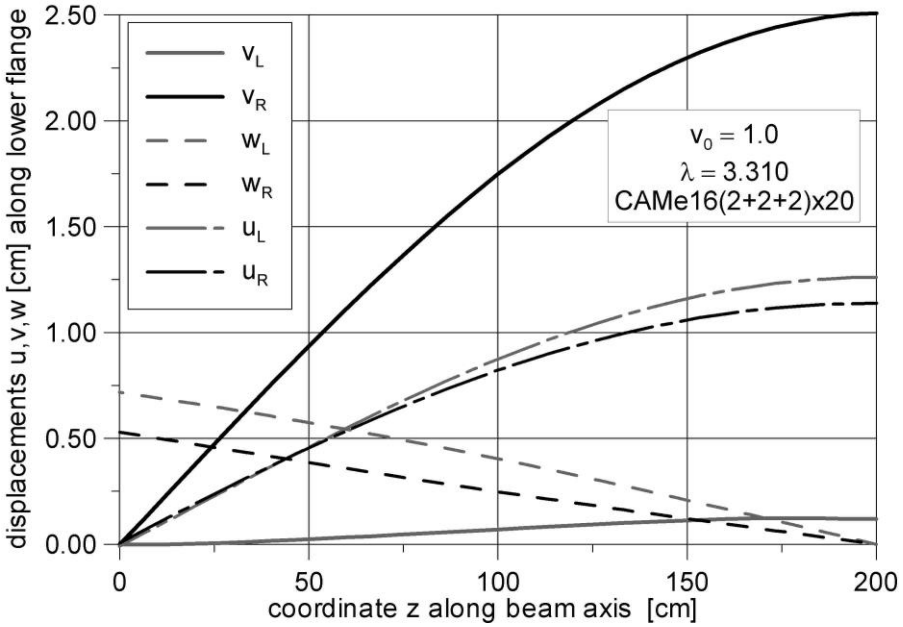

Fig. 10. Deformation of the lower flange (FEM): edge displacements along z-axis

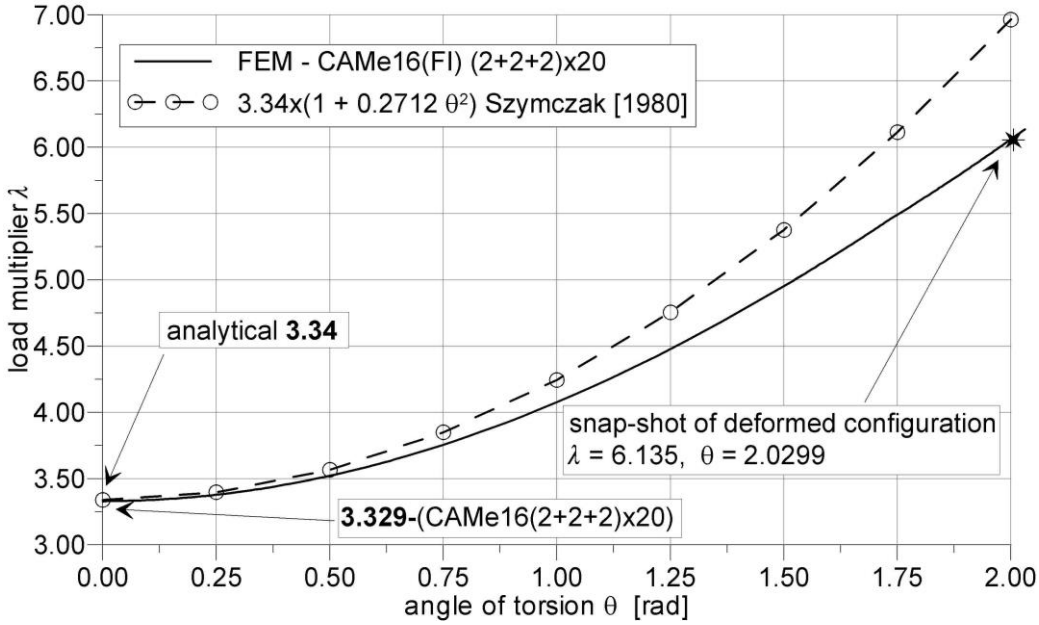

Fig. 11. Post-critical equilibrium paths after torsional buckling

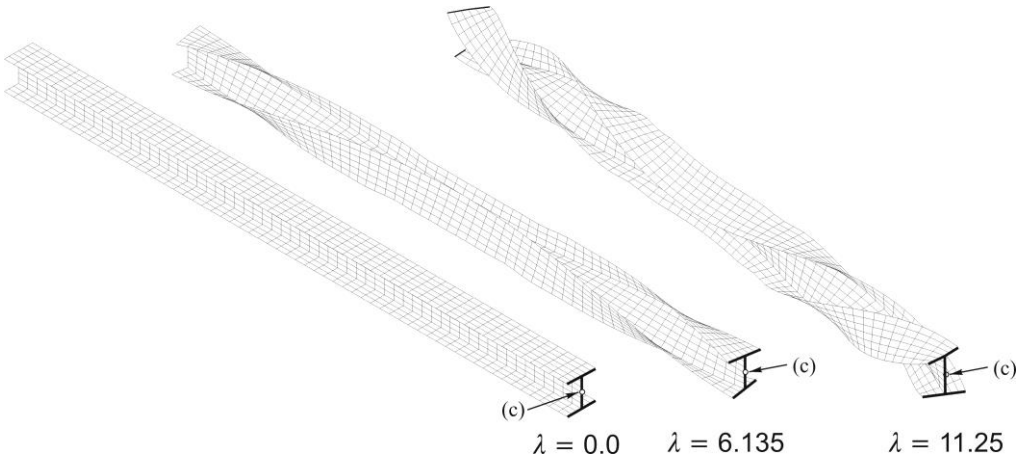

Fig. 12. Deformed beam in post-critical regime

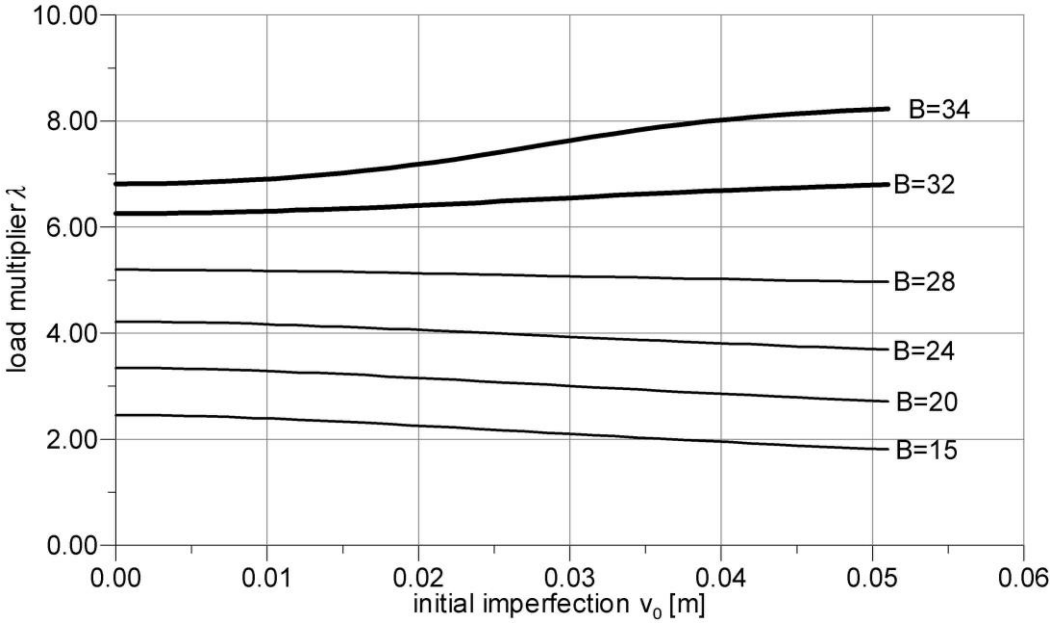

Fig. 13. Critical load vs initial imperfection for different flange widths

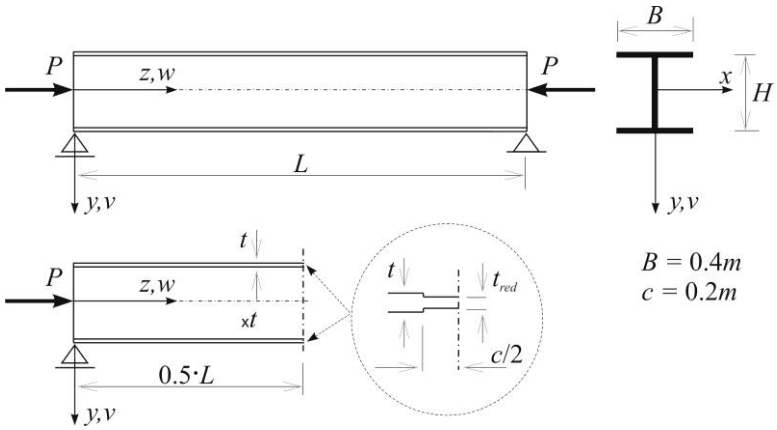

Fig. 14. I-beam column with notch – buckling mode localisation

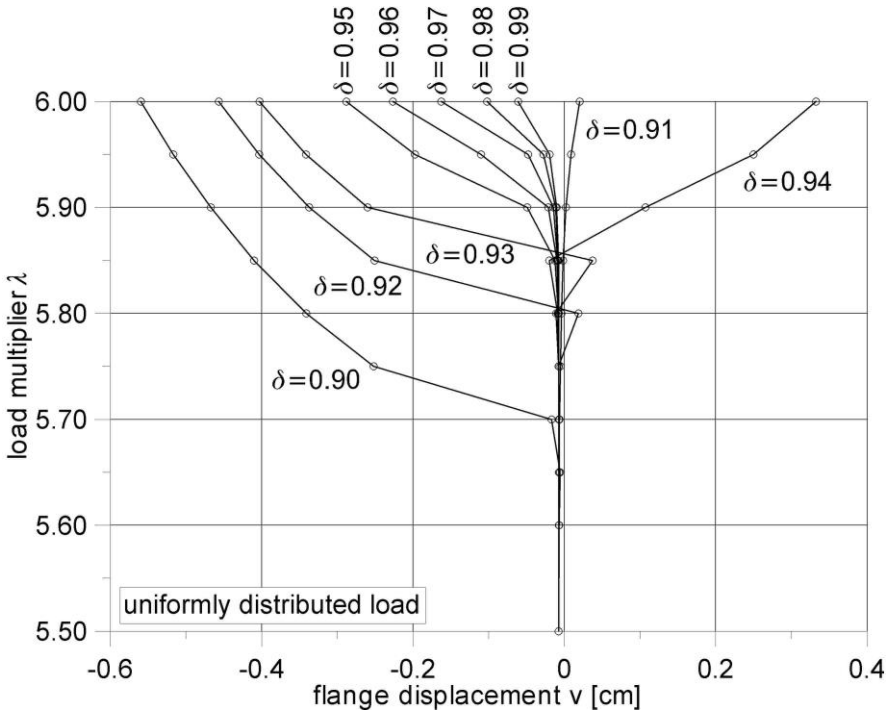

Fig. 15. Buckling mode localisation – equilibrium path for uniformly distributed load

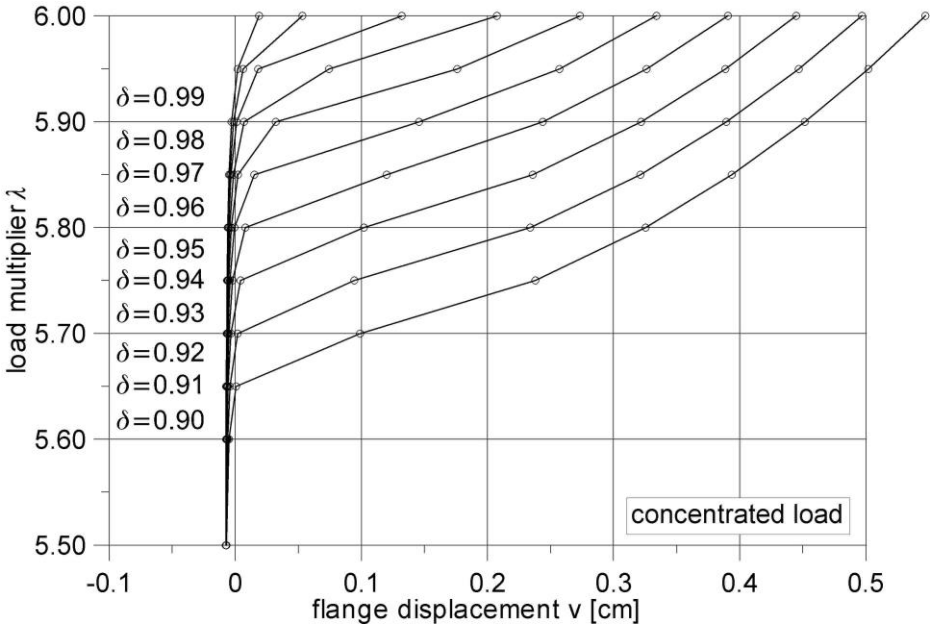

Fig. 16. Buckling mode localisation – equilibrium path for concentrated load

.

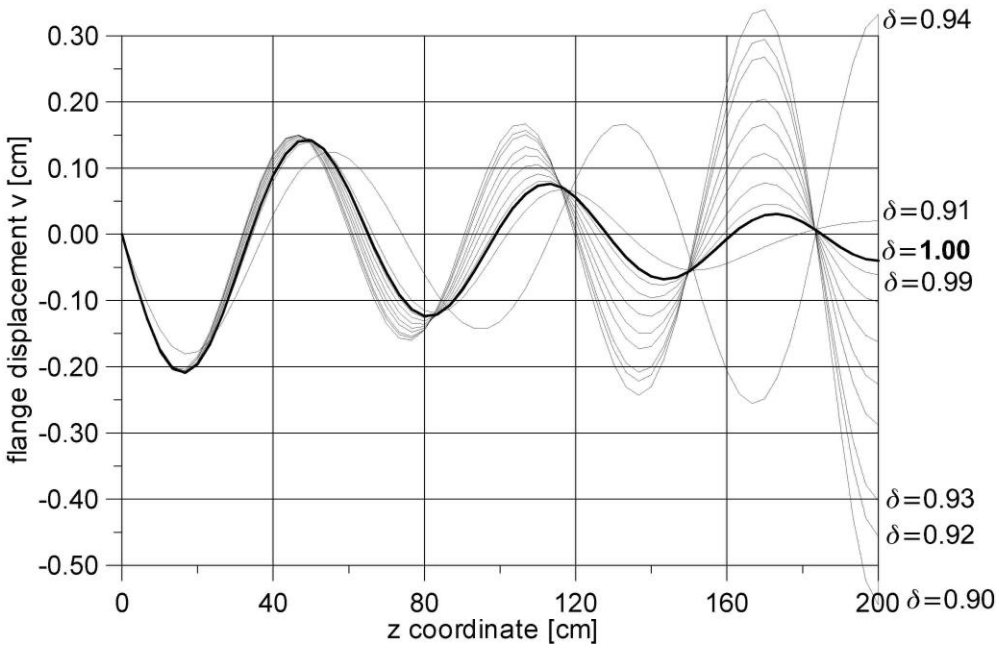

Fig. 17. Buckling mode localisation – vertical displacement of flange edge for uniformly distributed load

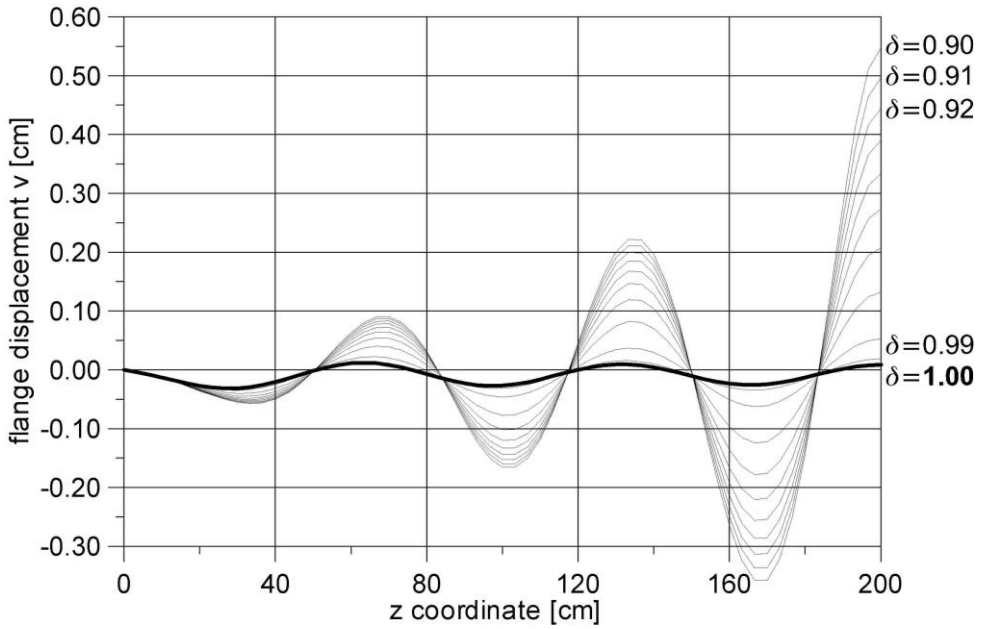

Fig. 18. Buckling mode localisation – vertical displacement of flange edge for concentrated load

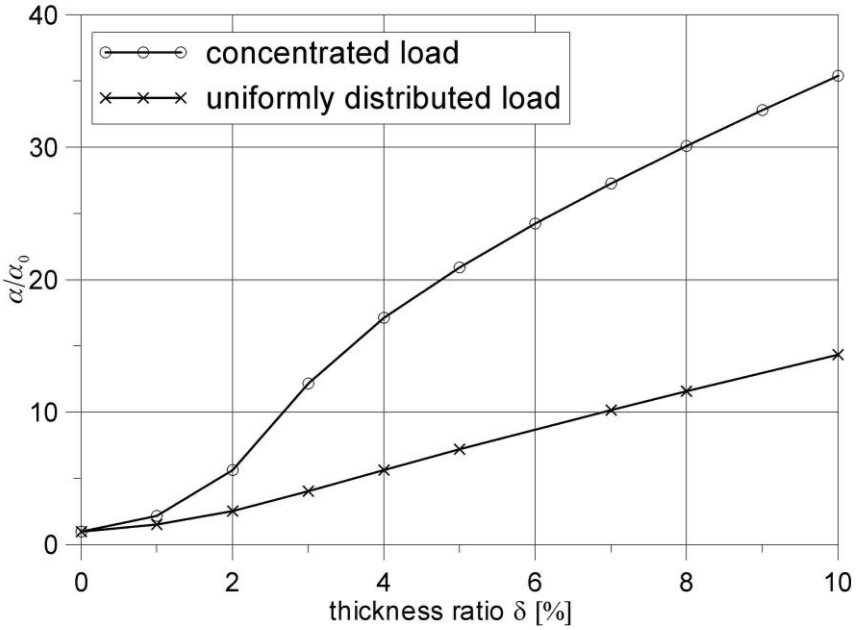

Fig. 19. Buckling mode localisation – ratio of amplitudes of the local buckling vs thickness reduction δ coefficient

Table 1. Convergence study

Element	Discretisation (elements) for whole beam	Number of degrees of freedom for ¼ of the beam	Critical torsional load P_{CR} MN
CAMe4(FI)	(2+2+2)×20	264	5.105
	(4+4+4)×40	882	3.775
	(6+6+6)×60	1860	3.529
	(8+8+8)×80	3198	3.442
CAMe9(FI)	(2+2+2)×20	882	3.337
	(4+4+4)×40	3198	3.330
CAMe16(FI)	(2+2+2)×20	1860	**3.329**
EAS14m1	(2+2+2)×20	264	3.36976
	(4+4+4)×40	882	3.33692
	(6+6+6)×60	1860	3.325
	(8+8+8)×80	3198	3.322
Szymczak [1]			3.343
Thimoshenko and Gere [5]			3.34